A New Kind of Accurate Calibration Method for Robotic Kinematic Parameters Based on the Extended Kalman and Particle Filter Algorithm

Zhihong Jiang, Weigang Zhou, Hui Li, Yang Mo, Wencheng Ni, and Qiang Huang, *Fellow, IEEE*

***Abstract*—Precise positioning of a robot plays an very important role in advanced industrial applications, and this paper presents a new kinematic calibration method based on the extended Kalman filter (EKF) and particle filter (PF) algorithm that can significantly improves the positioning accuracy of the robot. Kinematic and its error models of a robot are established, and its kinematic parameters are identified by using the EKF algorithm first. But the EKF algorithm has a kind of linear truncation error and it is useful for the Gauss noise system in general, so its identified accuracy will be affected for the highly nonlinear robot kinematic system with a non-Gauss noise system. The PF algorithm can solve this with non-Gauss noise and a high nonlinear problem well, but its calibration accuracy and efficiency are affected by the prior distribution of the initial values. Therefore, this paper proposes to use the calibration value of the EKF algorithm as the prior value of the PF algorithm, and then, the PF algorithm is used further to calibrate the kinematic parameters of the robot. Enough experiments have been carried out, and the experimental results validated the viability of the proposed method with the robot positioning accuracy improved significantly.**

***Index Terms*—Extended Kalman filter (EKF), non-Gauss noise, particle filter (PF), nonlinear system, robotic kinematic parameters calibration.**

I. Introduction

DUE TO factors such as machining tolerance, assembly tolerance, transmission clearance, and structural deformation, the actual kinematic and nominal kinematic parameters of a robot are different. This difference reduces robot positioning accuracy. However, robots require high positioning accuracy in precision operations and assembly tasks. Therefore, in order to enable positioning accuracy in precision operational tasks, it is necessary to accurately calibrate robot kinematics [1].

Previous research has been conducted on the calibration of robot kinematic parameters [2]–[4]. Abderrahim *et al.* [5] applied the rotating radius method based on the S-model of the rotation center and plane to accurately calibrate the kinematic parameters of a PUMA560 robot. A robot self-calibration method [6] was used to calibrate its kinematic parameters [7]–[9]. At the end effector of the robot, a flat or spherical constraint was applied; a constraint equation was then established to calibrate the robot's kinematic parameters. Chen *et al.* [10] proposed the exponential product model (POE) [11], [12], which is especially suitable for a reconfigurable robot [13]. Sun *et al.* calibrated the kinematic parameters of the robot through the vector loop method and the screw theory [14]. Although these methods can be used to calibrate the kinematic parameters of the robot and improve its positioning accuracy [15], [16], they fail to address the issues of high nonlinearity and significant measurement noise, which can both reduce robot calibration accuracy.

A nonlinear kinematic model for a robot is often linearized by ignoring second-order and above error terms. The least-square algorithm [17] is then used to identify the parameters of the kinematic model. Other algorithms also identify nonlinear kinematic parameters, such as the Levenberg–Marquardt algorithm [18], [19], Ridge estimation method [20], genetic algorithm [21], maximum likelihood estimation [22], [23], and extended Kalman filter (EKF) algorithm [24]. Omodei *et al.* [25] used the least-square algorithm, linear iterative algorithm, and EKF algorithm to identify the kinematic parameters of a SCARA robot, and then, compared the effectiveness of the three identification algorithms. When considering the influence of noise on the calibration system, EKF was observed to be the most effective algorithm because it more accurately identified the robot kinematic parameters [26]. The EKF algorithm deals with nonlinear systems that retain the Taylor expansion first-order terms of the nonlinear function and it ignores other higher order terms. It then uses the Kalman filter for filtering. The EKF algorithm is a suboptimal filter that cannot cope with a high nonlinear system. The main function of the algorithm is to approximate the nonlinear model with a linear model; it can only be applied to a Gaussian noise system [27]. The EKF algorithm does not work well on highly nonlinear and non-Gaussian noise systems.

Manuscript received June 11, 2017; revised July 29, 2017; accepted August 9, 2017. Date of publication August 31, 2017; date of current version January 5, 2018. This work was supported in part by the National Natural Science Foundation of China (61733001, 61573063, 61503029), in part by the National High Technology Research Plan of China (2015AA043101, 2015BAF10B02), and in part by the Basic Scientific Research of China (B2220133017). *(Corresponding authors: Zhihong Jiang and Hui Li.)*

The authors are with the School of Mechatronic Engineering, Beijing Institute of Technology, Beijing 100081, China (e-mail: jiangzhihong@bit.edu.cn; 1092175576@qq.com; lihui2011@bit.edu.cn; moyang602@163.com; nightswolf@qq.com; qhuang@bit.edu.cn).

Color versions of one or more of the figures in this paper are available online at http://ieeexplore.ieee.org.

Digital Object Identifier 10.1109/TIE.2017.2748058

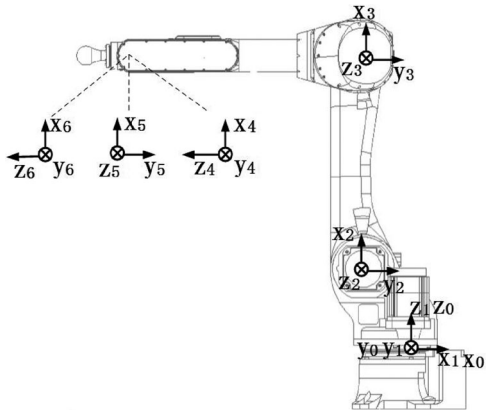

Fig. 1. Coordinate system for the RS10N robot.

However, nonlinear stochastic systems with non-Gaussian noise are very common in actual systems.

The robot kinematic model is a highly nonlinear system, with non-Gauss noise existing in the actual robot system. This paper proposes a new method for the calibration of robot kinematic parameters. First, the EKF is used to estimate the kinematic parameters of the robot. Next, the PF algorithm is used to deal with the nonlinear system, taking into account the effect of non-Gaussian noise. The kinematic model and the kinematic error model are established for an industrial robot with six degrees of freedom. The robot kinematic parameters are calibrated by the EKF, taking into account the influence of noise on kinematic parameters' identification in the calibration process. During the calibration process, errors occurred in the linear transformation as well as the non-Gaussian noise of the system. The calibration value of the EKF is used as the initial value; a set of random samples are then generated in the state space according to the prior distribution of the system state. These samples are used as the initial state of the particles and the PF algorithm is used to calibrate the kinematic parameters of the robot. Finally, improvements in robot positioning accuracy are analyzed after calibration.

The rest of this paper is organized as follows: Section II develops a kinematic model and a kinematic error model of the serial robot. In Section III, the robot kinematic parameters are preliminarily identified based on the EKF algorithm. Section IV applies the EKF and PF algorithm for accurate identification of kinematic parameters. The experimental results are shown in Section V, and the conclusions are presented in Section VI.

II. Robot Kinematic Model and Kinematic Error Model

Fig. 1 shows that each link coordinate system is established for the Kawasaki RS10N industrial robot. Table I lists the nominal D-H parameters of the robot. A kinematic model and a kinematic error model of the robot are established according to the Hartenberg–Denavit rule [28].

A link transformation matrix from link $i-1$ to link i can be described as (1). α is the link twist angle, a is the link length, d is the link offset, and θ is the joint angle [29].

TABLE I
Nominal Value of Kinematic Parameters

i	α_{i-1}/°	a_{i-1}/mm	d_i/mm	θ_i/°
1	0	0	0	θ_1
2	−90	99.5	0	θ_2
3	0	650.7	0	θ_3
4	90	0	700.2	θ_4
5	−90	0	0	θ_5
6	90	0	88	θ_6

$$\boldsymbol{A_i}=\begin{bmatrix} \cos\theta_i & -\sin\theta_i & 0 & a_{i-1} \\ \sin\theta_i\cos\alpha_{i-1} & \cos\theta_i\cos\alpha_{i-1} & -\sin\alpha_{i-1} & -\sin\alpha_{i-1}d_i \\ \sin\theta_i\sin\alpha_{i-1} & \cos\theta_i\sin\alpha_{i-1} & \cos\alpha_{i-1} & \cos\alpha_{i-1}d_i \\ 0 & 0 & 0 & 1 \end{bmatrix}. \tag{1}$$

The transformation matrix from the robot base coordinate to its end-effector coordinate is obtained by multiplying the link transformation matrices as follows:

$$\boldsymbol{T_6} = \boldsymbol{A_1}\boldsymbol{A_2}\boldsymbol{A_3}\boldsymbol{A_4}\boldsymbol{A_5}\boldsymbol{A_6}. \tag{2}$$

The D-H parameter deviations of each link results in transformation matrix errors. Taking into consideration the deviations, the transformation matrix can be expressed as

$$\begin{aligned}\boldsymbol{T_6}+\boldsymbol{\Delta T_6} = (\boldsymbol{A_1}+\boldsymbol{\Delta A_1})(\boldsymbol{A_2}+\boldsymbol{\Delta A_2})(\boldsymbol{A_3}+\boldsymbol{\Delta A_3}) \\ \times(\boldsymbol{A_4}+\boldsymbol{\Delta A_4})(\boldsymbol{A_5}+\boldsymbol{\Delta A_5})(\boldsymbol{A_6}+\boldsymbol{\Delta A_6}).\end{aligned} \tag{3}$$

The link transformation matrix error is approximately equal to the linear superposition of the D-H parameter deviations

$$\boldsymbol{\Delta A_i}=\frac{\partial \boldsymbol{A_i}}{\partial\alpha_{i-1}}\Delta\alpha_{i-1}+\frac{\partial \boldsymbol{A_i}}{\partial a_{i-1}}\Delta a_{i-1}+\frac{\partial \boldsymbol{A_i}}{\partial d_i}\Delta d_i+\frac{\partial \boldsymbol{A_i}}{\partial\theta_i}\Delta\theta_i \tag{4}$$

and (3) can be expanded as

$$\boldsymbol{T_6}+\boldsymbol{\Delta T_6}=\boldsymbol{A_1}\boldsymbol{A_2}\boldsymbol{A_3}\boldsymbol{A_4}\boldsymbol{A_5}\boldsymbol{A_6}+\boldsymbol{E_1}+\boldsymbol{E_2}+\cdots+\boldsymbol{E_6}. \tag{5}$$

In this paper, the D-H parameter deviations is very small. Therefore, the first-order error term $\boldsymbol{E_1}$ is the main consideration, $\boldsymbol{\Delta T_6}$ is approximately equal to $\boldsymbol{E_1}$ by ignoring the second- and higher order error terms ($\boldsymbol{E_2}\sim\boldsymbol{E_6}$) as follows:

$$\boldsymbol{\Delta T_6}\approx\boldsymbol{E_1}=\sum_{i=1}^{6}(\boldsymbol{A_1}\boldsymbol{A_2}\ldots\boldsymbol{A_{i-1}}\boldsymbol{\Delta A_i}\boldsymbol{A_{i+1}}\ldots\boldsymbol{A_5}\boldsymbol{A_6}). \tag{6}$$

The first three lines of the last column of the matrix $\boldsymbol{\Delta T_6}$ can be denoted as $\boldsymbol{Y}$. The size of $\boldsymbol{Y}$ is 3×1 and it represents the position errors vector of the end effector in x, y, and z. The linear relationship between the position errors vector of the end effector and the D-H parameter deviations of each link is then

obtained [30].

$$\boldsymbol{Y} = \begin{bmatrix} \boldsymbol{J_{11}} & \boldsymbol{J_{12}} & \boldsymbol{J_{13}} & \boldsymbol{J_{14}} \end{bmatrix} \begin{bmatrix} \boldsymbol{\Delta\alpha} \\ \boldsymbol{\Delta a} \\ \boldsymbol{\Delta d} \\ \boldsymbol{\Delta\theta} \end{bmatrix} = \boldsymbol{JX}. \quad (7)$$

Each of $\boldsymbol{\Delta\alpha}$, $\boldsymbol{\Delta a}$, $\boldsymbol{\Delta d}$, and $\boldsymbol{\Delta\theta}$ contains six parameters because the robot has six joints. $\boldsymbol{J}$ is a coefficient matrix that is only related to the nominal D-H parameters of the robot and $\boldsymbol{X}$ represents the deviations of the robot kinematic parameters.

$$\boldsymbol{X} = \begin{bmatrix} \boldsymbol{\Delta\alpha}^T & \boldsymbol{\Delta a}^T & \boldsymbol{\Delta d}^T & \boldsymbol{\Delta\theta}^T \end{bmatrix}^T. \quad (8)$$

The aforementioned equations are identified by the linear least-squares estimation (LSE) algorithm to obtain the D-H parameters of the robot. Although the LSE algorithm is a fast and efficient algorithm that can be used to solve a nonlinear equation [31], it is also very sensitive to noise. Therefore, in order to obtain higher parameter identification accuracy, the EKF is used to identify the nonlinear system with noise [32].

III. Preliminary Identification of Robot Kinematic Parameters Based on the EKF Algorithm

A laser tracker can measure the robot end-effector's position. Through the Jacobian matrix ($\boldsymbol{J}$) and position errors of the end effector, robot kinematic parameter deviations are computed. Due to the influence of noise, the EKF algorithm is used to identify the robot kinematic parameters. EKF is used as an optimization algorithm [33], [34] and it is applied to estimate the accurate deviations of D-H parameters by using these measured position values [35]. In the EKF algorithm, the $\boldsymbol{X}$ represents the deviations of the robot kinematic parameters, which is the same as that in Section II. Covariance matrix $\boldsymbol{P}$ can be expressed as

$$\boldsymbol{X_{k|k-1}} = \boldsymbol{X_{k-1|k-1}} \quad (9)$$

$$\boldsymbol{P_{k|k-1}} = \boldsymbol{P_{k-1|k-1}} + \boldsymbol{Q_{k-1}}. \quad (10)$$

$\boldsymbol{Q_{k-1}}$ is the covariance matrix of the system noise at the $(k-1)$th iteration. The position errors $\boldsymbol{Y_k}$ is obtained by measuring the end-effector's position of the robot through the laser tracker.

$$\boldsymbol{Y_k} = \boldsymbol{J_k X_k} + \boldsymbol{E_k}. \quad (11)$$

$\boldsymbol{E_k}$ represents the measurement error and $\boldsymbol{R_k}$ is the covariance matrix of the measurement noise at the kth iteration. The size of $\boldsymbol{X_k}$ is 24×1 at the kth iteration, it contains four groups of D-H parameter deviations, each group has six parameters because the robot has six joints and the size of the matrix $\boldsymbol{J_k}$ is 3×24; the Kalman gain can be expressed as

$$\boldsymbol{K_k} = \boldsymbol{P_{k|k-1}} \boldsymbol{J_k}^T \left(\boldsymbol{J_k P_{k|k-1}} \boldsymbol{J_k}^T + \boldsymbol{R_k} \right)^{-1}. \quad (12)$$

The optimal estimation value of $\boldsymbol{X}$ at the kth iteration is calculated by

$$\boldsymbol{X_{k|k}} = \boldsymbol{X_{k|k-1}} + \boldsymbol{K_k}(\boldsymbol{Y_k} - \boldsymbol{J_k X_{k|k-1}}). \quad (13)$$

Updating the covariance matrix $\boldsymbol{P}$ now gives

$$\boldsymbol{P_{k|k}} = (\boldsymbol{I} - \boldsymbol{K_k J_k}) \boldsymbol{P_{k|k-1}}. \quad (14)$$

The $k|k-1$ represents a prior estimate at the measurement point k, and $k|k$ represents a post estimate. $\boldsymbol{I}$ is the unit matrix, and the matrices $\boldsymbol{R}$ and $\boldsymbol{Q}$ for the EKF can be calculated by the method described in [36] and [37]. According to the aforementioned algorithm, the optimal robot kinematic parameter deviations are estimated at the kth iteration. The actual kinematic parameters ($\boldsymbol{X_R}$) of the robot are calculated by summing the values of the nominal kinematic parameters ($\boldsymbol{X_N}$) of the robot and the identification of the parameter deviations ($\boldsymbol{X}$).

$$\boldsymbol{X_R} = \boldsymbol{X_N} + \boldsymbol{X}. \quad (15)$$

The EKF algorithm uses the first order of the Taylor expansions to linearize the nonlinear system, and then, uses the Kalman filter to deal with the linear system. The identification accuracy is reduced due to linear transformation and non-Gaussian noise. However, the PF algorithm adequately solves the nonlinear system with non-Gaussian noise. The calibration accuracy and efficiency of the PF algorithm is affected by prior distributions of the initial value. Therefore, kinematic parameters calibrated by the EKF algorithm are again used as the initial value of the PF to accurately calibrate the robot kinematic parameters.

IV. Accurate Identification of Kinematic Parameters Based on the PF Algorithm

The preliminary calibration through the EKF algorithm is used to obtain a set of kinematic parameters. Using this set of parameters as the initial value of the PF algorithm, the PF algorithm converges quickly and effectively and also more accurately identify the kinematic parameters.

The error matrix of the robot kinematic parameters can be expressed as (8). The state-transition equation of the system is given as

$$\boldsymbol{X_k} = \boldsymbol{X_{k-1}} + \boldsymbol{U_k} \quad (16)$$

$$\boldsymbol{Z_k} = \boldsymbol{K}(\boldsymbol{X_N} + \boldsymbol{X_k}) - \boldsymbol{K}(\boldsymbol{X_N}) \quad (17)$$

$$\boldsymbol{K}(\boldsymbol{X_N}) = \boldsymbol{T_6} = \boldsymbol{A_1 A_2 A_3 A_4 A_5 A_6} \quad (18)$$

$$\boldsymbol{K}(\boldsymbol{X_N} + \boldsymbol{X_k}) = \boldsymbol{T_6} + \boldsymbol{\Delta T_6}. \quad (19)$$

$\boldsymbol{U_k}$ is the noise of the system; $\boldsymbol{Z_k}$ is the positioning error matrix of the robot's end effector; and K is the forward kinematics operator. The observation equation is a highly nonlinear system.

In accordance with the prior probability $p(\boldsymbol{X_0})$, the particles $\{\boldsymbol{X_k^i}\}$ are put into the state space. The superscript i represents the ith particle. The particle state value at the next moment is calculated by the state-transition equation of the system as follows:

$$\boldsymbol{X_k^i} = \boldsymbol{X_{k-1}^i} + \boldsymbol{U_k}. \quad (20)$$

The observation equation of the position error for each particle is given as

$$\boldsymbol{Z_k^i} = \boldsymbol{K}(\boldsymbol{X_N} + \boldsymbol{X_k^i}) - \boldsymbol{K}(\boldsymbol{X_N}). \quad (21)$$

The first three lines of the last column of the matrix $\boldsymbol{Z_k^i}$ can be denoted as $\boldsymbol{Y_k^i}$. The size of $\boldsymbol{Y_k^i}$ is 3×1 and it represents the position errors vector of the end effector in x, y, and z. In the

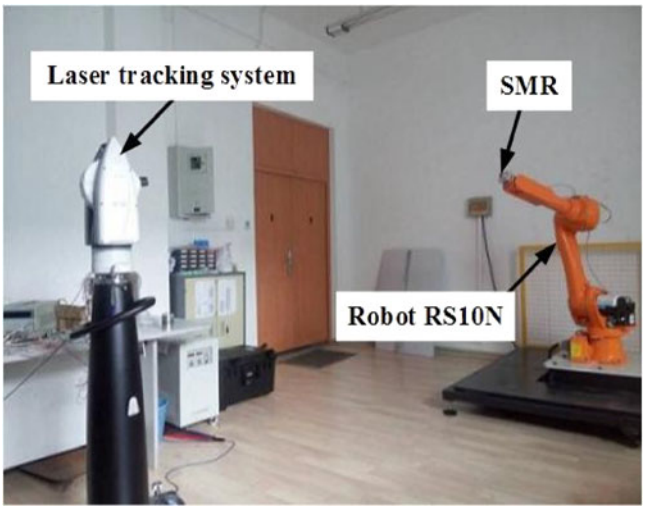

Fig. 2. Experimental system.

calibration process, the weight of the particle can be determined by the corresponding observation probability density, with the weight of the particle defined as

$$\omega_k^i = \frac{1}{\sqrt{2\pi\,|\boldsymbol{R}|}}\exp\left(-\frac{1}{2}\left[\boldsymbol{M_k}-\boldsymbol{Y_k^i}\right]^T\boldsymbol{R}^{-1}\left[\boldsymbol{M_k}-\boldsymbol{Y_k^i}\right]\right). \tag{22}$$

$\boldsymbol{M_k}$ is a vector of the position errors measured by the laser tracker and its size is 3×1 and $\boldsymbol{R}$ is the noise covariance matrix on the measurement process. The normalization of the particle weight is given as

$$\tilde{\omega}_k^i = \frac{\omega_k^i}{\sum_{j=1}^N \omega_k^j} \tag{23}$$

$$\boldsymbol{X_k} = \sum_{i=1}^{N}\tilde{\omega}_k^i\boldsymbol{X_k^i}. \tag{24}$$

In order to avoid the particle degradation, the particles are resampled according to their normalized weight. The low weight of the particles are removed and the high weight of the particles are copied [38]. The expectation of the particles can be calculated as (24).

The kinematic parameters of the robot are accurately identified through the aforementioned method. In the next section, experiments were conducted in order to verify the calibration of the robot under the new method.

V. Experiments and Results

The experimental object was a six-degrees-of-freedom Kawasaki RS10N industrial robot. The position of the robot's end effector was accurately measured by a Leica laser tracking system in order to validate the effectiveness of the algorithm [39]. Fig. 2 shows the experimental system.

In general, the base coordinate for a robot is established in the position of the first joint coordinate (see Fig. 1) or the center of the robot base frame. It is difficult to measure the exact location of the base coordinate; as such, it is also difficult to measure the absolute position of the end-effector coordinate relative to the

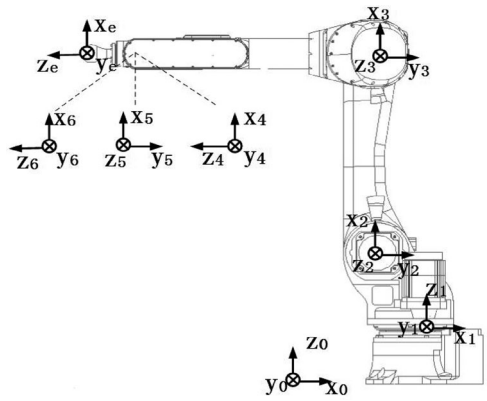

Fig. 3. New robot coordinate system.

robot base coordinate. During the experiment, the robot base coordinate was established on the outside of the robot and its position was measured by the laser tracker. Fig. 3 shows the relative relationship of the robot coordinate system.

Coordinate system 1 was relative to the position of the base coordinate system. An approximate value of this conversion relationship was obtained through the design parameters and was used as the nominal value of the D-H parameter. Next, spherically mounted retro reflectors (SMR) were installed at the robot's end effector. Its position coordinate system (relative to the sixth joint coordinate system) was calculated by matrix A_e. The position of the robot's end effector can be calculated as

$$\boldsymbol{T_e} = \boldsymbol{A_1}\boldsymbol{A_2}\boldsymbol{A_3}\boldsymbol{A_4}\boldsymbol{A_5}\boldsymbol{A_6}\boldsymbol{A_e}. \tag{25}$$

A total of 24 D-H parameters needed to be identified because the robot had six degrees of freedom. Also, three equations were provided for each measurement set of the end-effector's positions. The 24 D-H parameters needed to identify at least eight group equations. Adding more position measurements greatly improved the identification accuracy of the D-H parameters. When the measurements were sufficient, the D-H parameter deviations values tended to stabilize.

In general, the use of the EKF algorithm requires a trajectory, and the sampling interval is strict. In this system, enough points of the absolute position of the robot end effector are measured in the workspace, each point of the absolute position has an error. It is not along a trajectory, so the interval is not necessary. The absolute position of the end effector of the robot can be measured by the laser tracker and the predicted value of this position can be calculated through the nominal D-H parameters, so we can use the EKF algorithm to estimate the optimal value of the D-H parameters.

Two experiments were designed, with 100 end-effector's positions measured for each experiment. In the first experiment, the LSE and EKF algorithms were used to identify the corresponding D-H parameters. The covariance matrices of the EKF need to be setup with the initial values, both matrices Q and P are initialized by $10^{-4}\ I_{24\times 24}$ and the the matrix R is initialized by $10^{-4}\ I_{3\times 3}$ for the EKF algorithm and PF algorithm in the experiments. Then, taking the parameters identified by the EKF algorithm as the initial value of the PF algorithm, the robot D-H parameter deviations were accurately identified. Finally, the

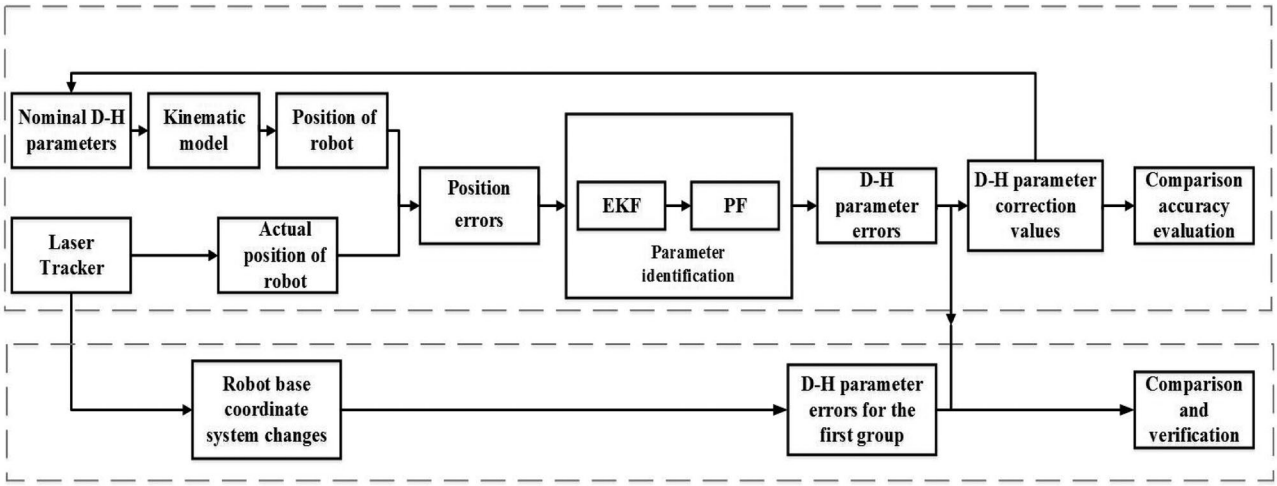

Fig. 4. Flow chart of calibration experiments.

TABLE II
ROBOT KINEMATIC PARAMETER DEVIATIONS

	LSE				EKF				EKF+PF			
Joint i	$\Delta\alpha_{i-1}$/°	Δa_{i-1}/mm	Δd_i/mm	$\Delta\theta_i$/°	$\Delta\alpha_{i-1}$/°	Δa_{i-1}/mm	Δd_i/mm	$\Delta\theta_i$/°	$\Delta\alpha_{i-1}$/°	Δa_{i-1}/mm	Δd_i/mm	$\Delta\theta_i$/°
1	0.494	0.5978	0.2073	0.1006	0.8594	3.5978	3.7073	0.2006	0.7894	2.4778	2.2523	−0.4506
2	−0.9897	−0.2926	0.4991	0.1000	−0.8997	1.6926	0.4991	0.3020	−0.7187	1.8226	−1.5632	0.2316
3	0.9429	−0.2939	0.2042	0.0996	0.7654	2.0939	0.2042	0.3996	0.5989	1.9139	1.2542	−0.7696
4	0.6015	−0.3054	0.4912	−0.0980	0.4015	−1.3054	0.4912	−0.5980	0.2815	−1.0854	2.0791	−0.2280
5	0.2003	−0.2958	0.1003	−0.1006	−0.3003	−1.4926	0.1003	−0.1006	−0.1703	−1.6858	−2.1603	0.6906
6	−0.4020	−0.2943	0.4120	0.1005	−0.2218	−0.2943	0.4120	0.1005	-0.2020	1.4343	0.9720	0.5525

positioning accuracy of the robot's end effector was analyzed after calibration. After the first experiment, the second experiment was carried out again to identify the D-H parameters when the base coordinate system was changed.

Fig. 4 shows the flow chart of the two experiments. Table II lists the deviations of the D-H parameters identified by the three algorithms for the first experiment. We need this results to calibrate the robot's D-H parameters. Next, we use the D-H parameters after calibrating to calculate the end-effector's position of the robot through the kinematics equation in (2) and we compare it with the position that is measured through the laser tracker. Finally, we can know the end-effector's position errors of the robot, so we can contrast the accuracy of the different methods. The EKF algorithm was used to identify the D-H parameters; the parameters were then used as the initial value of the PF algorithm. Fig. 5 shows the identification results of the 24 D-H parameter errors through the EKF + PF algorithm.

After the calibrations were completed through the three calibration algorithms, the robot positioning improvements were analyzed. A comparison of robot end-effector's positions (measured by the laser tracker and calculated by forward kinematics) shows improvements to end-effector's positioning accuracy. In the experiment, 50 positions were measured.

The position error Δe of the robot after experimental calibration through the methods has been compared in Fig. 6. And the Δe can be written as (26). Δx, Δy, and Δz represent the positioning errors of the robot's end effector in x–y–z directions.

$$\Delta e = \sqrt{(\Delta x)^2 + (\Delta y)^2 + (\Delta z)^2}. \tag{26}$$

It shows that the EKF algorithm adequately solved the influence of noise on the LSE algorithm in the calibration process. It also greatly improved the positioning accuracy of the robot's end effector. However, its calibration accuracy was lower than the PF algorithm. After completing the PF algorithm calibration, the end position error of the robot was reduced to a small range and the positioning accuracy was high. In the first experiment, the robot D-H parameters were corrected after calibration by the EKF + PF algorithm (see Table III).

In order to verify the effectiveness of the EKF + PF algorithm in the calibration experiment, a second calibration experiment was conducted. In the first experiment, the base coordinate system of the robot (base coordinate system 1) was in an external position where it could be accurately measured by the laser tracker. For the second experiment, the position of the robot base coordinate system was changed. The SMR was placed in a new position on the outside of the robot (base coordinate system 2). The new position was also measured by the laser tracker. The matrix transformation from base coordinate system 1 to base coordinate system 2 was calculated by the measured results of the laser tracker. Only the base coordinate system was changed; as such, the first group of D-H parameters was changed only

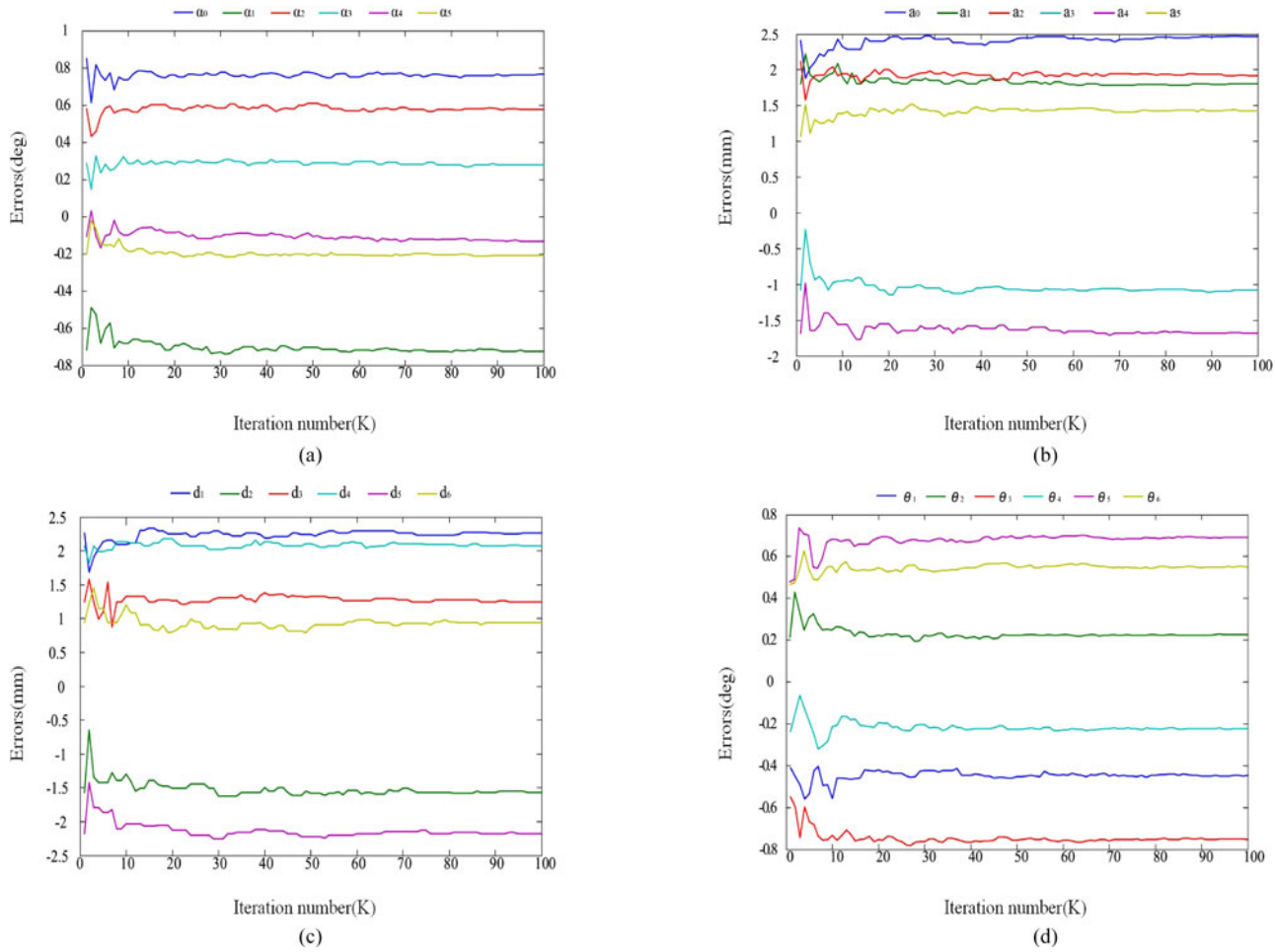

Fig. 5. Identified D-H parameter deviations through the EKF + PF algorithm.

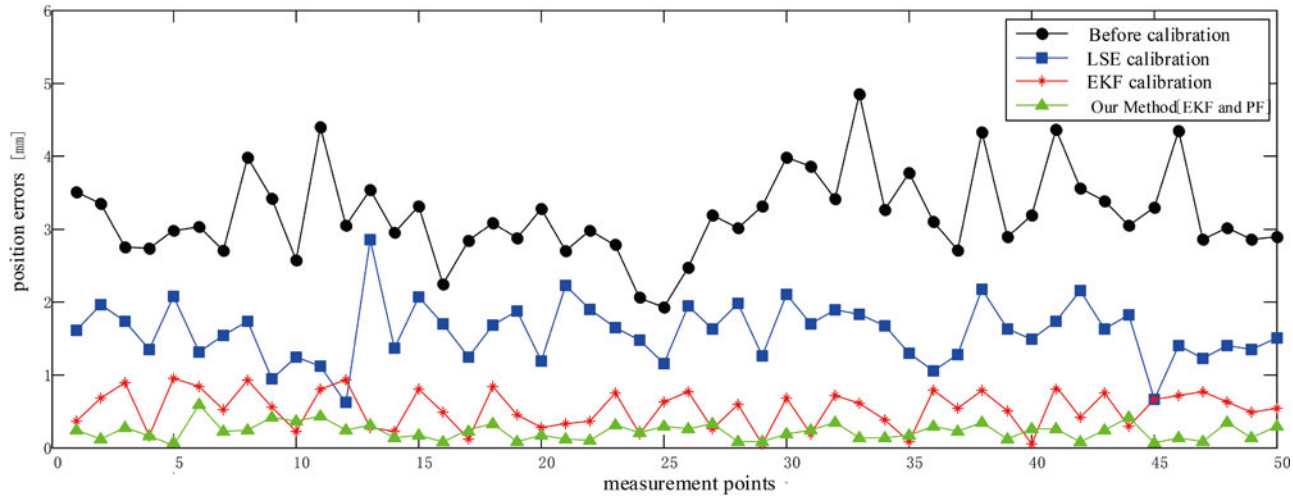

Fig. 6. Position errors of the robot after experimental calibration through the methods.

in theory. Changes to the first group of D-H parameters were taken as the robot D-H parameter deviations; however, changes could now be accurately measured by the laser tracker. Hundred robot end-effector's positions were measured and the robot D-H parameters were calibrated again through the EKF + PF algorithm (see Fig. 7).

Table IV lists the maximum values, average values, and mean square values of the position errors in the 50 groups of differ-

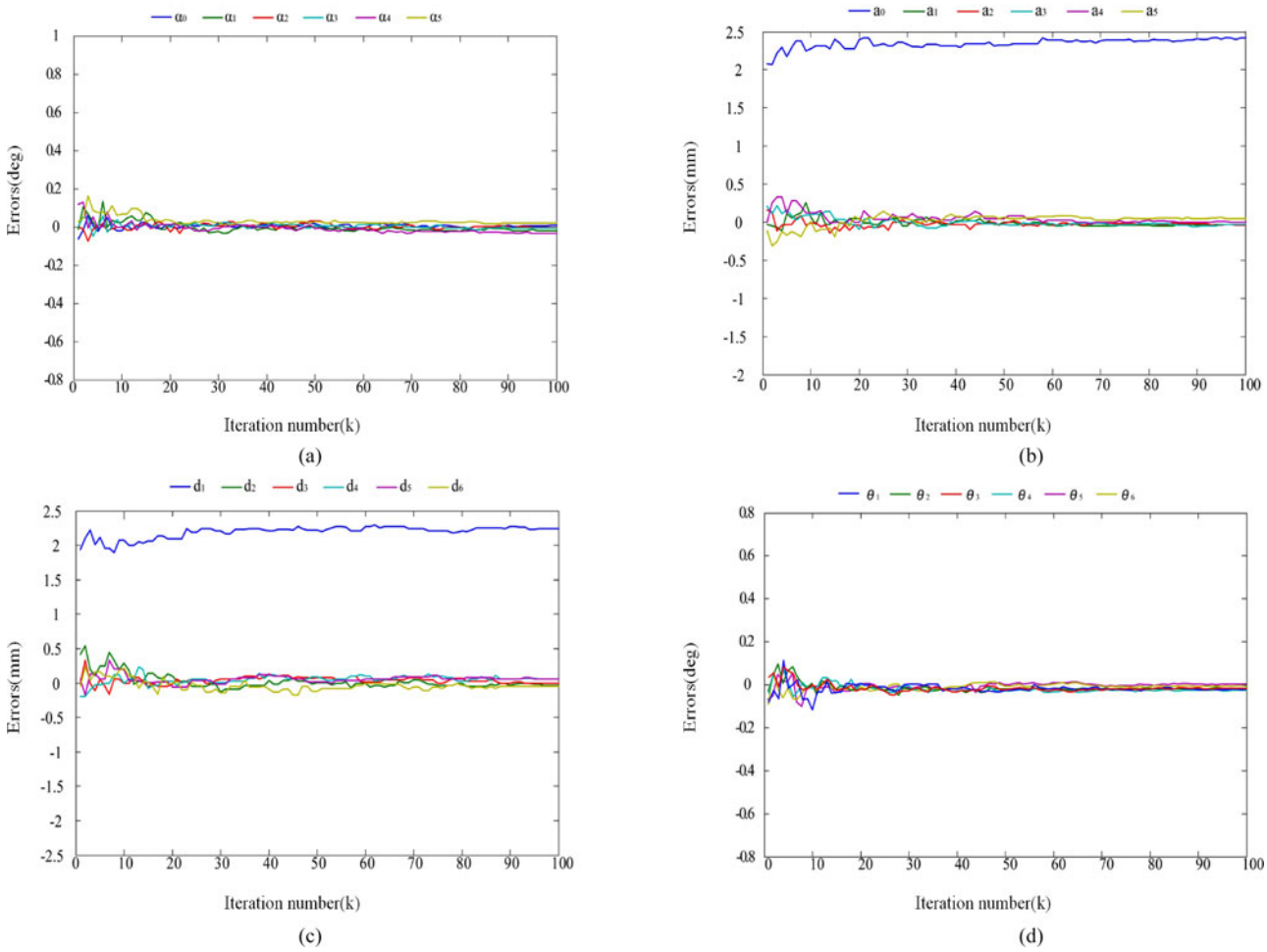

Fig. 7. Identification results of D-H parameter deviations after changing the base coordinate system.

TABLE III
ROBOT KINEMATIC PARAMETERS AFTER CALIBRATION

i	α_{i-1}/°	a_{i-1}/mm	d_i/mm	θ_i/°
1	0.7894	202.4778	432.2523	−0.4506
2	−90.7187	101.3226	−1.5632	0.2316
3	0.5989	652.6139	1.2542	−0.7696
4	90.2815	−1.0854	702.2791	−0.2280
5	−90.1703	−1.6858	−2.1603	0.6906
6	89.798	1.4343	88.972	0.5525

TABLE IV
ROBOT END-EFFECTOR POSITIONING ERRORS

	Mean (mm)	Std (mm)	Max (mm)
Before Calibration	3.1407	0.9332	4.8867
After LSE Calibration	1.6948	0.5424	2.7934
After EKF Calibration	0.5297	0.3218	0.9433
After EKF and PF Calibration	0.2621	0.1428	0.6421

ent joint angles of the robot. The experimental results showed that the robot kinematic parameter calibration method was accurate and effective. It greatly improved the absolute positioning accuracy of the robot's end effector, with the robot positioning error decreasing from 3.1407 to 0.2621 mm after calibration.

Here, only the first group of D-H parameters was changed compared to the first experimental calibration results, where the base coordinate system was changed. The changes agreed with the laser tracker measurements, with other D-H parameters groups almost unchanged. This fully verified the effectiveness and accuracy of the method.

VI. CONCLUSION

This paper presented a more accurate and effective method to calibrate the kinematic parameters of a robot. Based on the EKF algorithm providing priori value, the PF algorithm was used to successfully calibrate the robot kinematic parameters. The PF algorithm adequately solved the calibration accuracy problem caused by nonlinear and non-Gauss noise. For the two groups of experiments, the robot's end-effector positions were first measured, then the base coordinate system was changed and the positions were measured again to identify the kinematic parameters. The experimental results showed that the calibration method was effective and practical. The robot positioning accuracy greatly improved after the calibration.

In future work, the calibration algorithm will be applied to the kinematic model of other robots. Also, the online calibration and compensation method will be applied without stopping the robot, which may result in even great calibration efficiency.

References

[1] R. P. Judd and A. B. Knasinski, "A technique to calibrate industrial robots with experimental verification," *IEEE Trans. Robot. Autom.*, vol. 6, no. 1, pp. 20–30, Feb. 1990.

[2] S. Hayati and M. Mirmirani, "Improving the absolute positioning accuracy of robot manipulators," *J. Robot. Syst.*, vol. 2, no. 4, pp. 397–413, Dec. 1985.

[3] Z. Roth, B. Mooring, and B. Ravani, "An overview of robot calibration," *IEEE J. Robot. Autom.*, vol. 5, no. 3, pp. 377–385, Oct. 1987.

[4] P. L. Broderick and R. J. Cipra, "A method for determining and correcting robot position and orientation errors due to manufacturing," *J. Mechanisms, Transmiss., Autom. Design*, vol. 110, no. 1, pp. 3–10, Mar. 1988.

[5] M. Abderrahim and A. Whittaker, "Kinematic model identification of industrial manipulators," *Robot. Comput.-Integr. Manuf.*, vol. 16, no. 1, pp. 1–8, Feb. 2000.

[6] Y. Zhu, C. X. Hu, J. C. Hu, and K. M. Yang, "Accuracy and simplicity oriented self-calibration approach for two-dimensional precision stages," *IEEE Trans. Ind. Electron.*, vol. 60, no. 6, pp. 2264–2272, Jun. 2013.

[7] H. Zhuang, S. H. Motaghedi, and Z. S. Roth, "Robot calibration with planar constraints," in *Proc. IEEE Int. Conf. Robot. Autom.*, May 1999, vol. 1, pp. 805–810.

[8] A. Nubiola and I. A. Bonev, "Absolute robot calibration with a single telescoping ballbar," *Precision Eng.*, vol. 38, no. 3, pp. 472–480, Jul. 2014.

[9] J. Santolaria, F. J. Brosed, J. Velazquez, and R. Jimenez, "Self-alignment of on-board measurement sensors for robot kinematic calibration," *Precision Eng.*, vol. 37, no. 3, pp. 699–710, Jul. 2013.

[10] C. I-Ming, Y. Guilin, T. Chee, Tat, and Y. Song, Huat, "Local POE model for robot kinematic calibration," *Mechanism Mach. Theory*, vol. 36, no. 11–12, pp. 1215–1239, Nov. 2001.

[11] R. B. He, X. W. Li, T. L. Shi, and B. Wu, "A kinematic calibration method based on the product of exponentials formula for serial robot using position measurements," *Robotica*, vol. 33, no. 6, pp. 1295–1313, Jul. 2014.

[12] L. Wu, X. D. Yang, K. Chen, and H. L. Ren, "A minimal POE-based model for robotic kinematic calibration with only position measurements," *IEEE Trans. Autom. Sci. Eng.*, vol. 12, no. 2, pp. 758–763, Apr. 2015.

[13] Y. Guilin, C. I-Ming, L. Wee, Kiat, and H. Y. Song, "Self-calibration of three-legged modular reconfigurable parallel robots based on leg-end distance errors," *Robotica*, vol. 19, no. 2, pp. 187–198, Mar. 2001.

[14] T. Sun, P. Wang, B. Lian, S. Liu, and Y. Zhai, "Geometric accuracy design and error compensation of a one-translational and three-rotational parallel mechanism with articulated traveling plate," *Proc. Inst. Mech. Eng.*, Feb. 2017, doi: 10.1177/0954405416683433.

[15] Z. G. Fei, X. J. Xu, Y. Q. Xiao, N. Meier, and A. Georgiadis, "Kinematic self-calibration of non-contact five-axis measuring machine using improved genetic algorithm," *Meas. Sci. Technol.*, vol. 27, no. 2, p. 025903, Feb. 2016, doi: 10.1088/0957-0233/27/2/025903.

[16] T. Messay, R. Ordonez, and E. Marcil, "Computationally efficient and robust kinematic calibration methodologies and their application to industrial robots," *Robot. Comput.-Integr. Manuf.*, vol. 37, pp. 33–48, Feb. 2016.

[17] W. K. Veitschegger and C. H. Wu, "Robot calibration and compensation," *IEEE J. Robot. Autom.*, vol. 4, no. 6, pp. 643–656, Dec. 1988.

[18] M. Grotjahn, M. Daemi, and B. Heimann, "Friction and rigid body identification of robot dynamics," *Int. J. Solids Struct.*, vol. 38, no. 10–13, pp. 1889–1902, Mar. 2001.

[19] J. Shawash and D. R. Selviah, "Real-time nonlinear parameter estimation using the Levenberg-Marquardt algorithm on field programmable gate arrays," *IEEE Trans. Ind. Electron.*, vol. 60, no. 1, pp. 170–176, Jan. 2013.

[20] T. Sun, Y. Zhai, Y. Song, and J. Zhang, "Kinematic calibration of a 3-DOF rotational parallel manipulator using laser tracker," *Robot. Comput.-Integr. Manuf.*, vol. 41, pp. 78–91, Oct. 2016.

[21] Y. Song, J. Zhang, B. Lian, and T. Sun, "Kinematic calibration of a 5-DOF parallel kinematic machine," *Precision Eng.*, vol. 45, pp. 242–261, Jul. 2016.

[22] J. M. Renders, E. Rossignol, and M. Becquet, "Kinematic calibration and geometrical parameter identification for robots," *IEEE Trans. Robot. Autom.*, vol. 7, no. 6, pp. 721–732, Dec. 1991.

[23] H. Naruse, A. Nobiki, T. Yabuta, and M. Tateda, "High-accuracy multi-viewpoint stereo measurement using the maximum-likelihood method," *IEEE Trans. Ind. Electron.*, vol. 44, no. 4, pp. 571–578, Aug. 1997.

[24] A. Martinelli, N. Tomatis, and A. Tapus, "Simultaneous localization and odometry calibration for mobile robot," in *Proc. IEEE/RSJ Int. Conf. Intell. Robots Syst.*, Oct. 2003, vol. 1, pp. 1499–1504.

[25] O. Alberto, L. Giovanni, and A. Riccardo, "Three methodologies for the calibration of industrial manipulators: Experimental results on a SCARA robot," *J. Field Robot.*, vol. 17, no. 6, pp. 291–307, May 2000.

[26] R. Bucy and K. Senne, "Digital synthesis of non-linear filters," *Automatica*, vol. 7, no. 3, pp. 287–298, May 1971.

[27] K. Reif and R. Unbehauen, "The extended Kalman filter as an exponential observer for nonlinear systems," *IEEE Trans. Signal Process.*, vol. 47, no. 8, pp. 2324–2328, Aug. 1999.

[28] R. S. Hartenberg and J. Denavit, "A kinematic notation for lower pair mechanisms based on matrices," *J. Appl. Mech.*, vol. 77, no. 2, pp. 215–221, 1955.

[29] J. J. Craig, *Introduction to Robotics: Mechanics and Control* (ser. 10), vol. 4, 3rd ed. Pearson Education, New York, USA, Apr. 2005.

[30] W. Veitschegger and C. H. Wu, "Robot accuracy analysis based on kinematics," *IEEE J. Robot. Autom.*, vol. 2, no. 3, pp. 171–179, Sep. 1986.

[31] F. Ding, T. Chen, and L. Qiu, "Bias compensation based recursive least-squares identification algorithm for MISO systems," *IEEE Trans. Circuits Syst. II, Express Briefs*, vol. 53, no. 5, pp. 349–353, May 2006.

[32] Q. Huaming, H. Wei, and Q. Linchen, "Robust extended Kalman filter for attitude estimation with multiplicative noises and unknown external disturbances," *IET Control Theory Appl.*, vol. 8, no. 15, pp. 1523–1536, Oct. 2014.

[33] H. Y. Guo, H. Chen, F. Xu, F. Wang, and G. Y. Lu, "Implementation of EKF for vehicle velocities estimation on FPGA," *IEEE Trans. Ind. Electron.*, vol. 60, no. 9, pp. 3823–3835, Sep. 2013.

[34] M. Habibullah and D. D. Lu, "A speed-sensorless FS-PTC of induction motors using extended Kalman filters," *IEEE Trans. Ind. Electron.*, vol. 62, no. 11, pp. 6765–6778, Nov. 2015.

[35] I. W. Park, B. J. Lee, S. H. Cho, Y. D. Hong, and J. H. Kim, "Laser-based kinematic calibration of robot manipulator using differential kinematics," *IEEE/ASME Trans. Mechatronics*, vol. 17, no. 6, pp. 1059–1067, Dec. 2012.

[36] V. A. Bavdekar, A. P. Deshpande, and S. C. Patwardhan, "Identification of process and measurement noise covariance for state and parameter estimation using extended Kalman filter," *J. Process Control*, vol. 21, no. 4, pp. 585–601, Apr. 2011.

[37] G. Du and P. Zhang, "Online serial manipulator calibration based on multisensory process via extended Kalman and particle filters," *IEEE Trans. Ind. Electron.*, vol. 61, no. 12, pp. 6852–6859, Dec. 2014.

[38] B. F. Wu and C. L. Jen, "Particle filter based radio localization for mobile robots in the environments with low-density WLAN APs," *IEEE Trans. Ind. Electron.*, vol. 61, no. 12, pp. 6860–6870, Dec. 2014.

[39] M. Vincze, J. P. Prenninger, and H. Gander, "A laser tracking system to measure position and orientation of robot end effectors under motion," *Int. J. Robot. Res.*, vol. 13, no. 4, pp. 305–314, Aug. 1994.

Zhihong Jiang was born in Jiangsu, China. He received the B.S. degree in material processing/manufacturing engineering from the Jilin Technology of University, Changchun, China, in 1998, the M.S. degree in material processing/manufacturing engineering from Jilin University, Changchun, China, in 2001, and the Ph.D. degree in electrical engineering and automation from Tsinghua University, Beijing, China, in 2005.

He is currently an Associate Professor with the School of Mechatronic Engineering, Beijing Institute of Technology, Beijing. His research interests include space intelligent robotics, industry robot system, artificial intelligence and robot vision, and human computer interaction.

Weigang Zhou was born in Hubei, China. He received the B.S. degree in mechatronic engineering from the Beijing Institute of Technology, Beijing, China, in 2015, where he is currently working toward the M.S. degree with the School of Mechatronic Engineering.

His research interests include robot trajectory planning, servo control system, and accurate calibration.

Hui Li was born in Hebei, China. He received the B.S. degree in mechatronic engineering from the Hebei University of Technology, Tianjin, China, in 2005, the M.S. degree in mechatronic engineering from the Harbin Institute of Technology, Harbin, China, in 2007, and the Ph.D. degree in mechatronic engineering from the Beijing Institute of Technology, Beijing, China, in 2011.

He is currently a Lecture with the School of Mechatronic Engineering, Beijing Institute of Technology. His research interests include intelligent robotics, industry robot system, artificial intelligence, and robot vision.

Yang Mo was born in Hunan, China. He received the B.S. degree in mechatronic engineering and the M.S. degree in mechanical engineering from the Beijing Institute of Technology, Beijing, China, in 2013 and 2016, respectively, where he is currently working toward the Ph.D. degree with the School of Mechatronic Engineering.

His research interests include robot vision, servo control system, and intelligent robotics.

Wencheng Ni was born in Jiangxi, China. He received the B.S. degree in mechanical engineering from the Beijing Institute of Technology, Beijing, China, in 2009, where he is currently working toward the Ph.D. degree with the School of Mechatronic Engineering.

His research interests include robot arm, dexterous hand, and mechanism design.

Qiang Huang (M'98–SM'14–F'16) was born in Hubei, China. He received the B.S. and M.S. degrees in electrical engineering from the Harbin Institute of Technology, Harbin, China, in 1986 and 1989, respectively, and the Ph.D. degree in mechanical engineering from Waseda University, Tokyo, Japan, in 1996.

He was a Research Fellow with the National Institute of Advanced Industrial Science and Technology, Tokyo, between 1996 and 1999. He was a Research Fellow with the University of Tokyo, Tokyo, between 1999 and 2000. He is currently a Professor with the Beijing Institute of Technology, Beijing, China. He is the Director of Intelligent Robotics Institute, and the Director of the Key Laboratory of Biomimetic Robots and Systems, Ministry of Education of China.

Prof. Huang received First Class Prize of Ministry of Education Award for Technology Invention. He serves as chairs in many IEEE conferences, such as the organizing committee chair of the 2006 IEEE/RSJ International Conference on Intelligent Robots and Systems, and the general chair of the 2017 IEEE International Conference on Robotics and Biomimetics and the 2018 IEEE-RAS International Conference on Humanoid Robotics.